Active Management of LV Residential Networks under High PV Penetration

S.M.N.R. Abadi, M. Mahmoodi, P. Scott, L. Blackhall, S. Thiebaux
College of Engineering and Computer Science, The Australian National University
Canberra, Australia
Emails: (mahdi.noori, masoume.mahmoodi, paul.scott, lachlan.blackhall, sylvie.thiebaux)@anu.edu.au

***Abstract*—Active network management through residential owned devices, such as battery systems and smart inverters, has been introduced as a promising solution to mitigate voltage issues caused by rooftop solar. Existing decentralized approaches to determining setpoints for these devices, require network visibility and timed coordination to consider the impact of multiple control actions prescribed simultaneously by different controllers. To address this issue, we propose an online decentralized rule-based control approach, which prevents overvoltage/undervoltage by determining dynamic setpoints of PV smart inverters and battery systems, based on online measured connection point voltage. In the proposed method, successive control actions ensure that the voltage gradually converges to the desired region, and coordination between controllers occurs implicitly via the power system. The effectiveness of the proposed method is assessed on a real 30-bus feeder and achieves results that are within 4% of those obtained by a centralised multi-period AC OPF with perfect forecast.**

***Index Terms*—Active network management, Battery systems, Distribution networks, Decentralized voltage control, Smart inverters**

I. Introduction

In the last decade, the growing adoption of photovoltaic (PV) rooftop panels has led to new challenges in distribution systems operation [1]. Maximum PV generation often coincides with low residential load consumption, which necessitates the injection of power into the electric grid and in turn raises distribution voltages potentially beyond safe limits [2]. To alleviate the voltage rise problem, traditional approaches suggest grid reinforcement which is costly, and the use of on-load tap changer (OLTC) which can decrease the transformers life span [3]. Utilization of smart inverters and residential battery systems (henceforth battery), can be an effective alternative as they reduce the investment cost and provide fast and dynamic response [4-5].

PV active power injection to the network can be reduced using batteries and/or active power curtailment capability of smart inverters [2,6]. While the costs of batteries have decreased in recent years, it is still expensive to have enough battery capacity to absorb all the surplus PV power [7]. On the other hand, active power curtailment effectively throws away surplus renewable generation, reducing the value to PV owners [8]. To compensate, reactive power consumption provided by smart inverters can decrease the required active power curtailment, at the expense of increasing network losses [7]. Combining all three of these techniques can produce a better outcome, but given these trade-offs it can be challenging to find the best action in each instance. The challenge increases further still when solving the problem at a network level with many connected systems.

This paper presents a fully decentralized solution to this voltage control problem, that achieves near-to the same performance of an optimally controlled central system, but without the complexity. Control approaches for smart inverter and battery are divided into three categories: centralized, distributed and decentralized (i.e. local) [9]. Unlike decentralized control approaches, centralized and distributed approaches require communication and suffer from privacy concerns [10]. In decentralized approaches, control actions are decided only based on local measurements [11]. These approaches mainly focus on the regulation of the PV active and reactive power outputs based on voltage magnitude [12]. A simple method is the adoption of a fixed limit on the injected active power of PV to the network, which is defined based on the trade-offs between technical benefits and effects on PV owners [2,16]. However, this limitation is determined based on the worst-case scenario, which may happen once a year and therefore is very conservative. Also, this method does not employ the full potential of fast and dynamic capability of smart inverters and batteries.

Another approach is to utilize piece-wise linear Volt/VAR and Volt/Watt curves of smart inverters using instantaneous local voltage mismatch as input. The use of rule-based algorithms to efficiently utilize piece-wise linear curves is investigated in [5,11-15]. The voltage sensitivity matrix obtained from solved power flow, provides an accurate way to calculate droop slopes. In [14], droop coefficients are calculated based on a voltage sensitivity matrix to share active power curtailment equally among all PV inverters. In [11], droop coefficients are updated in each period using the voltage sensitivity matrix to avoid errors associated with fixed sensitivity factors. However, updating a voltage sensitivity matrix requires full observability of the network and remote monitoring. To overcome the need of remote monitoring, [12] proposed a fitting function-based sensitivity approach that develops a nonlinear function to describe dependencies between the voltage of a bus and its PV active and reactive power injections

978-1-5386-4722-6/19/$31.00 ©2019 IEEE

and then calculates the slopes based on the function. This function does not account for the control actions of other buses and time delays are defined to coordinate the control actions. However, defining time delays could be complicated for large networks and they should be altered if the network configuration changes. All the aforementioned literature try to calculate the exact active and reactive powers required to bring the voltage to the desired region in each instance, and therefore suffer from a) underutilization of resources in order to ensure system stability [17] either, b) unnecessary utilization of reactive power or active power curtailment due to the lack of active management of multiple simultaneously occurring control actions.

In this paper, the proposed decentralized rule-based control approach, instead of calculating the exact active and reactive powers required, employs a small portion in each control action. Therefore, the voltage gradually converges towards the desired region through each control action. In this way, small changes in active/reactive powers ensure the stability of local controllers and also, it eliminates the need for communication or time delays to coordinate the control actions of controllers as the coordination between controllers occurs implicitly via the power system. Smart inverters and local voltage measurements are fast enough to perform sufficient control actions to bring voltage to desired region. The proposed control approach consists of three modes of operation, Mode 1 is activated when the connection point voltage exceeds the desired region and is responsible for battery charging, reactive power consumption and active power curtailment to bring the connection point voltage to the desired region. Mode 2 is activated when the connection point voltage is lower than the desired region and is responsible for discharging the battery and reactive power injection. Mode 3 is activated when the voltage is within the desired region and is responsible for normal operation and restoration of active/reactive power. To assess the effectiveness of the proposed method, we carry out a comparison with an ideal centralized multi-period AC optimal power flow which has perfect information about realization of uncertainty.

II. Voltage Deviation and Droop Control Method

In this section overvoltage caused by reverse power flow, and the use of piece-wise linear curves for active and reactive power management are briefly described. Fig. 1 shows a simple two-bus system where extra active PV power is injected to the grid. This injected power may produce a voltage rise at the point of common coupling which can be approximated [3] by:

$$V_N - V_G = \frac{RP_N + XQ_N}{V_N} \tag{1}$$

where V_N is the voltage at the connection point, *R* and *X* areresistance and reactance of the line between the two buses, P_N and Q_N are the injected active and reactive powers from the connection point to the grid, respectively. To decrease voltage deviation, injected active and reactive powers could be managed. It is assumed that PV and battery are connected to the grid via separated inverters and that the batterys inverter is working in unity power factor.

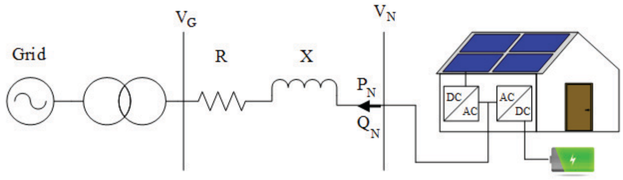

Fig. 1. A simple two bus feeder

A. Active Power Management

Injected active power could be managed through batteries utilization, by charging the batteries with the extra PV active power generation or active power curtailment, or by controlling the output power of the PV inverter. One way to implement active power management is using droop control methods in which, injected active power is calculated as a function of voltage at the connection point. In this method, the battery will be charged or the PV inverter will curtail the active power only when the connection point voltage is higher than the upper desired limit (V_3), shown in Fig. 2, and also the battery will be discharged when the voltage is lower than the lower desired limit (V_2). Fig. 2.a and 2.b show the schematic of changes in AC solar output and charge/discharge of the battery as a function of the measured voltage at the connection point, respectively. In these figures, V_1 and V_4 are used to adjust the slopes of the curves and P_{MPP} is the maximum active power that can be obtained through the PV inverter.

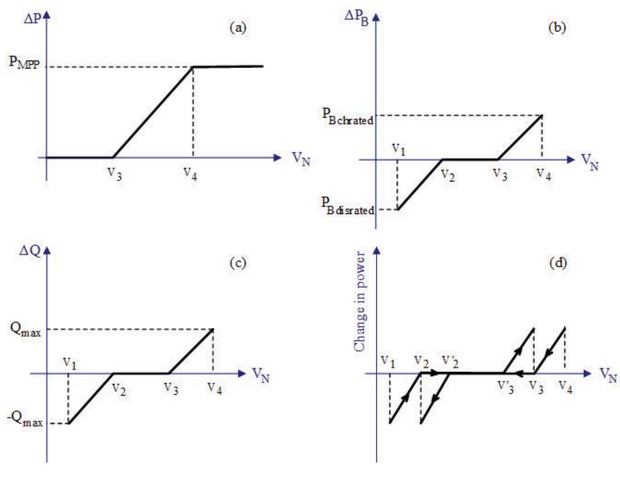

Fig. 2. The schematics of local active and reactive powers management; a) change in PV active power curtailment; b) change in charge/discharge of the battery; c) change in inverter reactive power injection/consumption; d) hysteresis curves for restoration mode

B. Reactive power management

As stated in [7], due to high reactance of *MV/LV* distribution transformers, the cumulative R/X ratio is not so high, and as a result, the reactive power could have a large effect on voltage regulation. However, it should be considered that a large amount of reactive power can increase losses and require higher power rating inverters [8]. Droop control methods can also be used for reactive power management of residential PV inverters. Reactive power consumption/injection for mitigating overvoltage/undervoltage is determined as a function of voltage in the connection point, shown in Fig. 2.c. In this figure V_2 and V_3 are the lower and upper desired voltage limits, V_1 and V_4 are used to adjust the slopes of the curve and Qmax is the maximum amount of reactive power limited by the inverter size and active output power of PV.

III. Proposed Control Method

In this section, we propose a decentralized rule-based control method which consists of three modes of operation. In each control mode, charging and discharging of the battery, and active and reactive powers of the PV inverter are determined based on the online measurements of the local connection point voltage. As summarized in Section I, based on the measured voltage, one of the modes of controller will be activated. The details of each mode are described in the following paragraphs.

A. Mode 1: Overvoltage

When the connection point voltage exceeds the upper desired limit (V_3), battery increasingly charges as a function of its connection point voltage as (2), until its active charging power reaches the maximum charging rate or bring the connection point voltage to the desired region. The battery is charged based on the calculated amount until it is fully charged.

$$P_B(t) = \begin{cases} min(P_B(t-1) + m_1(V(t) - V_3), P_{Bchrated}) \ \ if \\ \hfill SOC(t-1) \leq SOC_{max} \\ 0, \hfill \text{otherwise.} \end{cases} \tag{2}$$

$$SOC(t) = SOC(t-1) + \eta_{ch} P_B(t) \tag{3}$$

where $P_B(t)$ is the active power of the battery in each time step that positive and negative amounts show charging and discharging of the battery, respectively, m_1 is the droop coefficient obtained from the slope of the curve in Fig 2.b, $V(t)$ is the online measured connection point voltage, $P_{Bchrated}$ is the maximum rate of charge of the battery, SOC is the state of charge of the battery, $SOC(t-1)$ is the state of charge of the battery in previous time step and SOC_{max} is the battery size and η_{ch} is the batterys charging efficiency.

If the battery reaches its maximum charging rate but the overvoltage persists, the inverter reactive power consumption increasingly adjusts as a function of its connection point voltage, as shown in (4), until either it reaches its maximum amount, limited by the apparent power of the inverter or the voltage is mitigated.

$$Q_{PV}(t) = \begin{cases} min(Q_{PV}(t-1) + m_2(V(t) - V_3), Q_{max}) \ \ if \\ P_B(t-1) = P_{Bchrated} \ or \ SOC(t-1) = SOC_{max}. \\ 0, \hfill \text{otherwise.} \end{cases} \tag{4}$$

where $Q_{PV}(t)$ is the inverter reactive power in each time step that positive and negative amounts show consumption and injection of the battery, respectively. m2 is the droop coefficient obtained from the slope of the curve in Fig 2.c and Q_{max} is the maximum amount of reactive power which is limited by the inverter size and the active output power of PV.

If the battery and reactive power consumption could not alleviate the overvoltage, the active output power is curtailed as a function of its connection point voltage (5). Since normally the voltage deviation is larger for buses located at the end of the feeder, according to (2) and (4), the rates of battery charge and reactive power consumption in these buses are larger values. Therefore, they reach $P_{Bchrated}$ and Q_{max} sooner than the other buses, and hence, they start to curtail active power sooner. To use the full potential of other buses and avoid unnecessary active power curtailment in buses located at the end of the feeder, another starting criteria, *A*, is defined. For each bus, *A* is true when the voltage deviation is smaller than a threshold or the voltage exceeds the upper desired limit for a number of consecutive time steps. The threshold and the number of consecutive time steps are obtained based on trial and error method.

$$P_{PV}(t) = \begin{cases} min(P_{PV}(t-1) + m_3(V(t) - V_3), 0) \hfill if \\ \hfill Q_{PV}(t-1) = Q_{max} \ and \ A = true \\ P_{PV}(t-1), \hfill \text{otherwise.} \end{cases} \tag{5}$$

where $P_{PV}(t)$ is the inverter active output power in each time step and m_3 is the droop coefficient obtained from the slope of the curve in Fig 2.a.

B. Mode 2: Undervoltage Mode

As stated in [18], inverters are capable to inject reactive power to the grid to alleviate undervoltage during peak load time, which happens simultaneously with low PV active power generation. When the connection point voltage is smaller than the lower desired limit (V_2), the battery increasingly discharges as a function of its connection point voltage in each time step as (6), until it reaches its maximum discharge rate or brings the connection point voltage to the desired region. The battery is discharged based on the calculated amount until it is fully discharged.

$$P_B(t) = \begin{cases} max(P_B(t-1) + m_4(V(t) - V_2), P_{Bdisrated}) \ \ if \\ \hfill SOC(t-1) \geq 0 \\ 0, \hfill \text{otherwise.} \end{cases} \tag{6}$$

$$SOC(t) = SOC(t-1) + \frac{P_B(t)}{\eta_{dis}} \tag{7}$$

where m_4 is the droop coefficient obtained from the slope of the curve in Fig 2.b and $P_{Bdisrated}$ is the maximum rate of discharge of the battery which has a negative value. If the battery reaches its maximum discharging rate but the undervoltage persists, then the inverter reactive power increasingly adjusts as a function of its connection point voltage as shown in (8), until either it reaches its maximum amount, limited by the apparent power of the inverter, or the voltage is mitigated. m5 is the droop coefficient obtained from the slope of the curve in Fig 2.c.

$$Q_{PV}(t) = \begin{cases} max(Q_{PV}(t-1) + m_5(V(t) - V_2), -Q_{max}) \ \ if \\ \hfill P_B(t-1) = P_{Bdisrated} \ or \ SOC(t-1) = 0 \\ 0, \hfill \text{otherwise.} \end{cases} \tag{8}$$

C. Mode 3: Restoration

When the connection point voltage is within the desired region, we check whether curtailment has been applied in previous time steps in order to avoid unnecessary curtailment and harvest as much energy as possible from the PV. If so, the hysteresis curve in Fig. 2.d is used to prevent oscillation of voltage around upper desired limit. According to (9), the potential extra active PV power gradually augments as a function of the connection point voltage, as shown in Fig. 2.d. The process of active power restoration continues until it reaches P_{MPP} or the voltage reaches upper desired limit.

$$P_{PV}(t) = \begin{cases} min(P_{PV}(t-1) + m_3(V(t) - V_3), P_{MPP}) & \textit{if} \\ & P_{PV}(t-1) \leq P_{MPP} \\ P_{PV}(t-1), & \text{otherwise.} \end{cases} \tag{9}$$

If the active output power of the PV reaches its P_{MPP} and the voltage is still smaller than the upper desired limit, then to avoid unnecessary reactive power consumption, the extra reactive power is gradually decreased according to (10) using the hysteresis curve. A similar approach is applied to prevent unnecessary charging of the battery, as shown in (11).

$$Q_{PV}(t) = \begin{cases} max(Q_{PV}(t-1) + m_2(V(t) - V_3), 0) \ \ \textit{if} & \\ \qquad Q_{PV}(t-1) \geq 0 \ \textit{and} \ P_{PV}(t-1) = P_{MPP} & \\ 0, & \text{otherwise.} \end{cases} \tag{10}$$

$$P_B(t) = \begin{cases} max(P_B(t-1) + m_1(V(t) - V_3), 0) \ \ \textit{if} & \\ \qquad P_B(t-1) \geq 0 \ \textit{and} \ Q_{PV}(t-1) = 0 & \\ P_B(t-1), & \text{otherwise.} \end{cases} \tag{11}$$

Similarly, another hysteresis curve is defined to prevent unnecessary reactive power injection and battery discharging. The reactive power and battery discharge are restored according to (12) and (13), respectively.

$$Q_{PV}(t) = \begin{cases} min(Q_{PV}(t-1) + m_5(V(t) - V_2), 0) \ \ \textit{if} & \\ & Q_{PV}(t-1) \leq 0 \\ 0, & \text{otherwise.} \end{cases} \tag{12}$$

$$P_B(t) = \begin{cases} min(P_B(t-1) + m_4(V(t) - V_2), 0) \ \ \textit{if} & \\ & P_B(t-1) \leq 0 \\ P_B(t-1) & \text{otherwise.} \end{cases} \tag{13}$$

IV. AC Multi-Period Optimal Power Flow

To assess the effectiveness of the proposed method, we compare with a centralized multi-period AC optimal power flow. In this centralized AC-OPF, optimal charging/discharging of the batteries and active/reactive output power of the PVs are determined to minimize the cost of energy obtained from the upstream network:

$$OF = \min_{P_B, Q_{PV}, P_{PV}} \sum_t \lambda \times P_{upstream}(t) \tag{14.a}$$

subject to

$$f(P_{Bch}(t), P_{Bdis}(t), P_{PV}(t), Q_{PV}(t), P_L(t), V(t), \theta(t)) = 0 \tag{14.b}$$

$$V_{min} \leq V(t) \leq V_{max} \tag{14.c}$$

$$0 \leq P_{PV}(t) \leq P_{MPP} \tag{14.d}$$

$$P_{PV}^2(t) + Q_{PV}^2(t) \leq S_{max}^2 \tag{14.e}$$

$$SOC(t) = SOC(t-1) + \eta_{ch} P_{Bch}(t) - \frac{P_{Bdis}(t)}{\eta_{dis}} \tag{14.f}$$

$$0 \leq P_{Bch}(t) \leq P_{Bchrated} \tag{14.g}$$

$$0 \leq P_{Bdis}(t) \leq P_{Bdisrated} \tag{14.h}$$

$$0 \leq SOC(t) \leq SOC_{max} \tag{14.i}$$

where (14.a) shows the objective function in which λ is the electricity price, (14.b) stands for the power flow equations in which $P_L(t)$ is the active load power and $\theta(t)$ is the voltage angle at the connection point, (14.c) forces voltages to stay within the desired region, (14.d) and (14.e) indicate accepted amounts for active and reactive output powers of each PV based on P_{MPP} and the inverter size, and (14.f-14.i) show the batteries limitations. The multi-period AC-OPF is modelled as a non-linear programming problem and solved by commercial solver (CONOPT).

V. Results and Discussion

A. Case Study

We tested the performance of our proposed method using simulations on a real 30-bus modern underground LV feeder with $R/X \approx 2$ located in Hobart, Australia [19], in MATLAB/OpenDSS interface [20]. The LV feeder is shown in Fig. 3, and we consider a PV unit, a battery and a residential load at each bus. In our experiments, we model step changes in the load and solar every hour and the hourly PV generation and load consumption data are extracted from [21], as shown in Fig. 4. The often large instantaneous transitions between hours provide a good way to test the response of our control approach and allow us to clearly observe the settling time and behavior, given our 1 second controller voltage sampling rate. The controller and simulation parameters are summarized in Table I.

Fig. 5.a. shows the voltage profile at *Bus15* which is located at the end of the feeder with and without voltage management. When the voltage at Bus15 exceeds 1.05pu at 9am, Mode 1 of its controller is activated. The battery is increasingly charged based on (2) until it reaches its maximum charging rate after 12s, shown in Fig 5.b. However, as the overvoltage persists, the reactive power is increasingly consumed based on (3) until it brings the voltage to the desired region after 35s. At this time, Mode 3 is activated, but since the voltage is still more than the hysteresis range, the reactive power is not restored. As the overvoltage happens again at the beginning of the next hour, the reactive power consumption increases until it reaches to its maximum amount after 2s. At this stage, as described in section III.A, the controller waits to see the impact of other buses for 17s, and then it starts to curtail the active output power and increase the reactive power consumption subsequently. A similar strategy is applied for the next couple of hours until hour 15 in which the voltage enters the hysteresis range and the controller starts to restore active power curtailment based on (7). Within 39s the PV output power reaches P_{MPP} and then reactive power restoration starts based on

TABLE I
CONTROLLER AND SIMULATION PARAMETERS

Parameter	Value	Parameter	Value
V_1	0.8pu	PV inverter size	8kVA
V_2	0.95 pu	Battery inverter size	2kVA
V_2'	0.98pu	η_{ch}	80%
V_3'	1.02 pu	SOC_{max}	2kWh
V_3	1.05 pu	$P_{Bchrated}$	2kW
V_4	1.2 pu	$P_{Bdisrated}$	-2kW

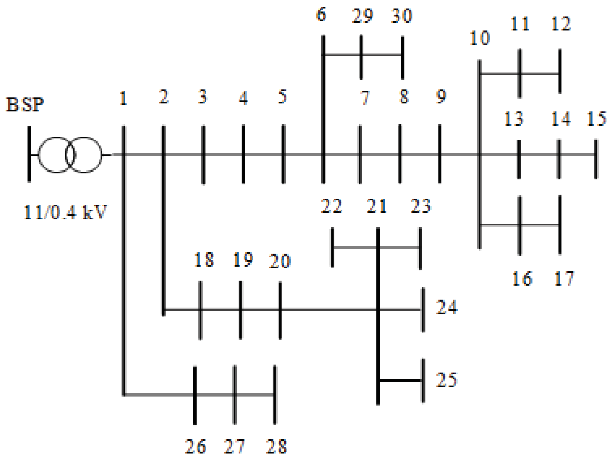

Fig. 3. 30-bus LV feeder

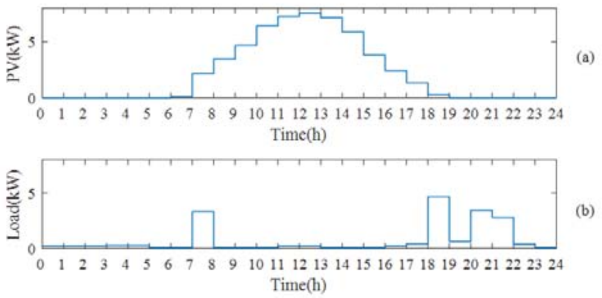

Fig. 4. a) PV power generation; b) residential load

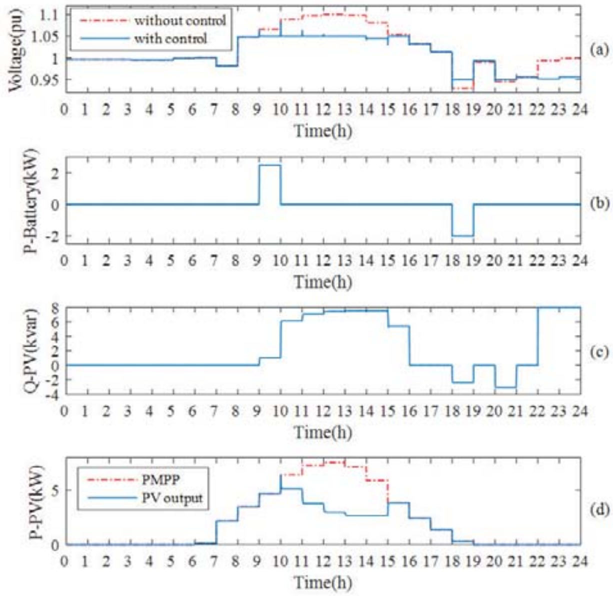

Fig. 5. Bus15: a) voltage profile with and without control; b) charge and discharge of the battery; c) reactive power; d) active power output and P_{MPP}

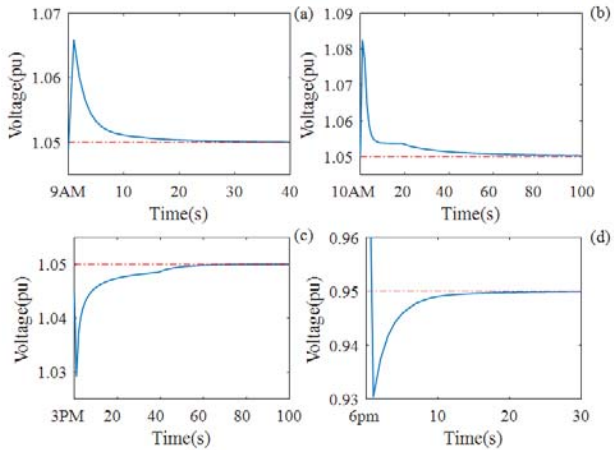

Fig. 6. Detailed performance of the proposed method for voltage of Bus15 at a) 9AM, mitigating overvoltage in 35s (12s increasing battery charging and 23s reactive power consumption). b) 10AM, mitigating overvoltage in 100s (2s increasing reactive power consumption, 17s waiting for the impact other buses and 81s increasing active power curtailment). c) 3PM, restoring active power curtailment in 39s and partial restoration of reactive power consumption in 21s. d) 6PM, mitigating undervoltage in 23s (5s increasing battery discharging and 18s increasing reactive power injection).

(8). The reactive power is completely restored within 12s at the beginning of the next hour. According to the load curve, peak demand happens at hour 18 which leads to undervoltage in Bus15. Therefore, Mode 2 of its controller is activated and the battery is increasingly discharged based on (5) until it reaches its maximum discharging rate after 5s. Then, reactive power injection starts increasing based on (6) until the voltage is brought back to the desired region. Similar process happens during the remaining hours. Fig. 6 demonstrates the detailed performance of the proposed method in hours 9,10,15 and 18 respectively. It can be seen that the controller reacts as soon as a change in load and generation data occurs and brings the voltage to the desired limit.

Fig. 7 shows the cost of the energy transferred between the LV feeder and the LV/MV transformer. Also, the results obtained from the multi-period AC-OPF is shown in this figure for comparison. Power flows from upstream to the feeder until 8am, as indicated by the positive amount, and reverses as indicated by the negative amount. The deviation between the cost of the ideal centralized approach and our proposed approach is 2.3%. The price of electricity is assumed constant throughout the day and for the sake of simplicity, we consider it to be 1$/kWh (this is equivalent to minimizing the net consumption of the feeder over time). It might be misleading as the cost associated with our proposed method is better than the optimal centralized AC-OPF between hours 11 until 14. In fact, since the ideal centralized AC-OPF is carried out under perfect forecast, the batteries are charged between these hours which lead to less active power injection to the network. The results show the effectiveness of the proposed local approach to follow the ideal central approach.

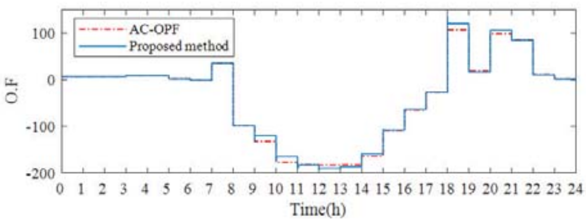

Fig. 7. Objective function

To further validate the efficacy of the proposed method, we consider different PV penetration scenarios. The results obtained by our method and AC-OPF are summarized in Table II. As the PV penetration increases, reactive power contribution of both AC-OPF and our method increase. However, the rate of increase in AC-OPF reactive power contribution is more than that of our proposed method, which leads to an increase in the relative difference between the harsh situations (end of the feeder), contribute less reactive power than with AC-OPF. Future work will consider enhancing their contribution by using different droop coefficients and voltage desired limits for different buses based on their location in the feeder.

VI. Conclusion

In this paper a novel decentralized rule-based control approach is proposed to mitigate overvoltage/undervoltage in a high PV penetrated distribution network, using residential batteries and smart inverters. Based on online measured connection point voltage, dynamic setpoints of PV smart inverters and batteries are determined, and the voltage converges toward the desired region gradually with each time step. The proposed approach consists of three modes of operation, overvoltage, undervoltage and restoration modes and each mode are responsible for a range of connection point voltage. The first two modes are activated to bring the voltage to the desired region and the third mode is defined to prevent unnecessary active power curtailment, reactive power consumption or injection and charge/discharge of the battery.

To assess the performance of the proposed approach to manage voltages, it was simulated on a real 30-bus high PV penetrated LV distribution network in Hobart, Australia. The results highlight that it has the potential to closely match the ideal centralized AC-OPF performance without the need of communication, full network observability, time delays and heavy offline computations.

A further extension would be to consider different droop coefficients and voltage desired limits for different buses based on their location in the feeder. This could ensure more contribution of buses which are not located at the end of the feeder and face less harsh voltage condition. Also, the use of algorithms such as model predictive control methods to periodically provide setpoints corrections for the proposed local control to better track the globally optimal solution.

TABLE II
Objective Function Values and Total Reactive Power for Different PV Penetration Scenarios

		PV ratio to the base scenario				
		1.2	1.1	1	0.9	0.8
Relative difference between objective functions		3.90%	3.80%	2.30%	1.10%	0.40%
Reactive power (kvarh)	Proposed method	261.3	212.4	163.5	122.3	82.9
	OPF	493.8	462.1	432.2	308.9	200.7

References

[1] A. Samadi, L. Sder, E. Shayesteh and R. Eriksson, "Static Equivalent of Distribution Grids With High Penetration of PV Systems," in IEEE Transactions on Smart Grid, vol. 6, no. 4, pp. 1763-1774, July 2015.

[2] S. Hashemi and J. stergaard, "Efficient Control of Energy Storage for Increasing the PV Hosting Capacity of LV Grids," in IEEE Transactions on Smart Grid, vol. 9, no. 3, pp. 2295-2303, May 2018.

[3] M. Zeraati, M. E. Hamedani Golshan and J. M. Guerrero, "Distributed Control of Battery Energy Storage Systems for Voltage Regulation in Distribution Networks With High PV Penetration," in IEEE Transactions on Smart Grid, vol. 9, no. 4, pp. 3582-3593, July 2018.

[4] S. W. Alnaser and L. F. Ochoa, "Optimal Sizing and Control of Energy Storage in Wind Power-Rich Distribution Networks," in IEEE Transactions on Power Systems, vol. 31, no. 3, pp. 2004-2013, May 2016.

[5] F. Olivier, P. Aristidou, D. Ernst and T. Van Cutsem, "Active Management of Low-Voltage Networks for Mitigating Overvoltages Due to Photovoltaic Units," in IEEE Transactions on Smart Grid, vol. 7, no. 2, pp. 926-936, March 2016.

[6] J. von Appen, T. Stetz, M. Braun and A. Schmiegel, "Local Voltage Control Strategies for PV Storage Systems in Distribution Grids," in IEEE Transactions on Smart Grid, vol. 5, no. 2, pp. 1002-1009, March 2014.

[7] P. H. Divshali and L. Sder, "Improving Hosting Capacity of Rooftop PVs by Quadratic Control of an LV-Central BSS," in IEEE Transactions on Smart Grid.

[8] Y. Wang, K. T. Tan, X. Y. Peng and P. L. So, "Coordinated Control of Distributed Energy-Storage Systems for Voltage Regulation in Distribution Networks," in IEEE Transactions on Power Delivery, vol. 31, no. 3, pp. 1132-1141, June 2016.

[9] K. Worthmann, C. M. Kellett, P. Braun, L. Grne and S. R. Weller, "Distributed and Decentralized Control of Residential Energy Systems Incorporating Battery Storage," in IEEE Transactions on Smart Grid, vol. 6, no. 4, pp. 1914-1923, July 2015.

[10] M. Zeraati, M. E. H. Golshan and J. M. Guerrero, "A Consensus-Based Cooperative Control of PEV Battery and PV Active Power Curtailment for Voltage Regulation in Distribution Networks," in IEEE Transactions on Smart Grid.

[11] T. Sansawatt, L. F. Ochoa and G. P. Harrison, "Smart Decentralized Control of DG for Voltage and Thermal Constraint Management," in IEEE Transactions on Power Systems, vol. 27, no. 3, pp. 1637-1645, Aug. 2012.

[12] Z. Zhang, L. F. Ochoa and G. Valverde, "A Novel Voltage Sensitivity Approach for the Decentralized Control of DG Plants," in IEEE Transactions on Power Systems, vol. 33, no. 2, pp. 1566-1576, March 2018.

[13] Y. Xu, Z. Y. Dong, R. Zhang and D. J. Hill, "Multi-Timescale Coordinated Voltage/Var Control of High Renewable-Penetrated Distribution Systems," in IEEE Transactions on Power Systems, vol. 32, no. 6, pp. 4398-4408, Nov. 2017.

[14] R. Tonkoski, L. A. C. Lopes and T. H. M. El-Fouly, "Coordinated Active Power Curtailment of Grid Connected PV Inverters for Overvoltage Prevention," in IEEE Transactions on Sustainable Energy, vol. 2, no. 2, pp. 139-147, April 2011.

[15] H. S. Bidgoli and T. Van Cutsem, "Combined Local and Centralized Voltage Control in Active Distribution Networks," in IEEE Transactions on Power Systems, vol. 33, no. 2, pp. 1374-1384, March 2018.

[16] T. R. Ricciardi, K. Petrou, J. Franco and L. F. Ochoa, "Defining Customer Export Limits in PV-Rich Low Voltage Networks," in IEEE Transactions on Power Systems.

[17] H. Zhu and H. J. Liu, "Fast Local Voltage Control Under Limited Reactive Power: Optimality and Stability Analysis," in IEEE Transactions on Power Systems, vol. 31, no. 5, pp. 3794-3803, Sept. 2016.

[18] R. K. Varma, V. Khadkikar and R. Seethapathy, "Nighttime Application of PV Solar Farm as STATCOM to Regulate Grid Voltage," in IEEE Transactions on Energy Conversion, vol. 24, no. 4, pp. 983-985, Dec. 2009.

[19] Provided by TasNetworks.

[20] Available online: http://download2.nust.na/pub4/sourceforge/e/el/ electricdss/OpenDSS/OpenDSSManual.pdf

[21] Available online: http://www.lboro.ac.uk/research/crest/demand-model/